Structure, Volume *22*

Supplemental Information

HIV-1 Envelope Protein gp41: An NMR Study of Dodecyl Phosphocholine Embedded gp41 Reveals a Dynamic Prefusion Intermediate Conformation

Nils-Alexander Lakomek, Joshua D. Kaufman, Stephen J. Stahl, and Paul T. Wingfield

Supplemental Information Inventory

Figure S1, related to Results section “Monomer-Trimer Equilibrium” and Figure 4. The figure shows the sedimentation equilibrium centrifugation results for gp41$^{27\text{-}154}$ and the related loop deleted gp41 LD, in the presence and absence of DPC. All the profiles are fitted to a monomer - trimer equilibrium.

Figure S2, related to the Results “Monomer-Trimer Equilibrium” and Figure 4. The figure shows the mole percentage of monomer and trimer species as a function of total protein concentration for all the various gp41 constructs. The profiles were calculated from the data shown in Figure S1.

Figure S3, related to the Results section “Comparison of gp41$^{27\text{-}194}$ and gp41$^{1\text{-}194}$ including the fusion peptide” and Figure 1. The figure shows a comparison of ^{1}H, ^{15}N chemical shifts and $\Delta\delta^{13}C^{\alpha}$ secondary chemical shifts of gp41$^{1\text{-}194}$ compared to gp41$^{27\text{-}194}$.

Figure S4, related to the Results section “Comparison of gp41$^{27\text{-}194}$ and gp41$^{1\text{-}194}$ including the fusion peptide” and Figure 2. The figure shows the full list of ^{15}N relaxation data recorded for gp41$^{1\text{-}194}$ in DPC micelles (Lakomek et al., 2013) including additional resonances that could be newly assigned in the 2D spectra based on comparison to gp41$^{27\text{-}194}$.

Figure S5, related to the Results section “Comparison of gp41$^{27\text{-}194}$ and gp41$^{1\text{-}194}$ including the fusion peptide” and Figure 2. The figure shows a comparison of ^{15}N relaxation data recorded for gp41$^{27\text{-}194}$ compared to those for gp41$^{1\text{-}194}$.

Table S1, related to the Results section “Secondary structure analysis” and Figure 1. This table lists the $\Delta\delta^{13}C^{\alpha}$ secondary chemical shift for gp41$^{27\text{-}194}$.

Table S2, related to the Results section “Inter-domain dynamics” and Table 1. The table describes the input average relaxation data and back-calculated relaxation data for quality assessment of the fit.

Table S3, related to the Experimental Procedures section “NMR spectroscopy” and Figure 1. This table provides the backbone chemical shift assignments for the studied gp41$^{27\text{-}194}$ construct in DPC micelles.

Table S4, related to the Results section “Inter-domain dynamics” and Figure 2. This table provides the full list of ^{15}N relaxation data for gp41$^{27\text{-}194}$, measured at 600 MHz and 800 MHz.

Table S5, related to the Results section **“**Lipid interactions and solvent-accessibility” and Figure 3. This table provides the full list of lipid (5-DSA) and solvent (Omniscan) PRE data.

Supplemental Data

Supplemental Figures

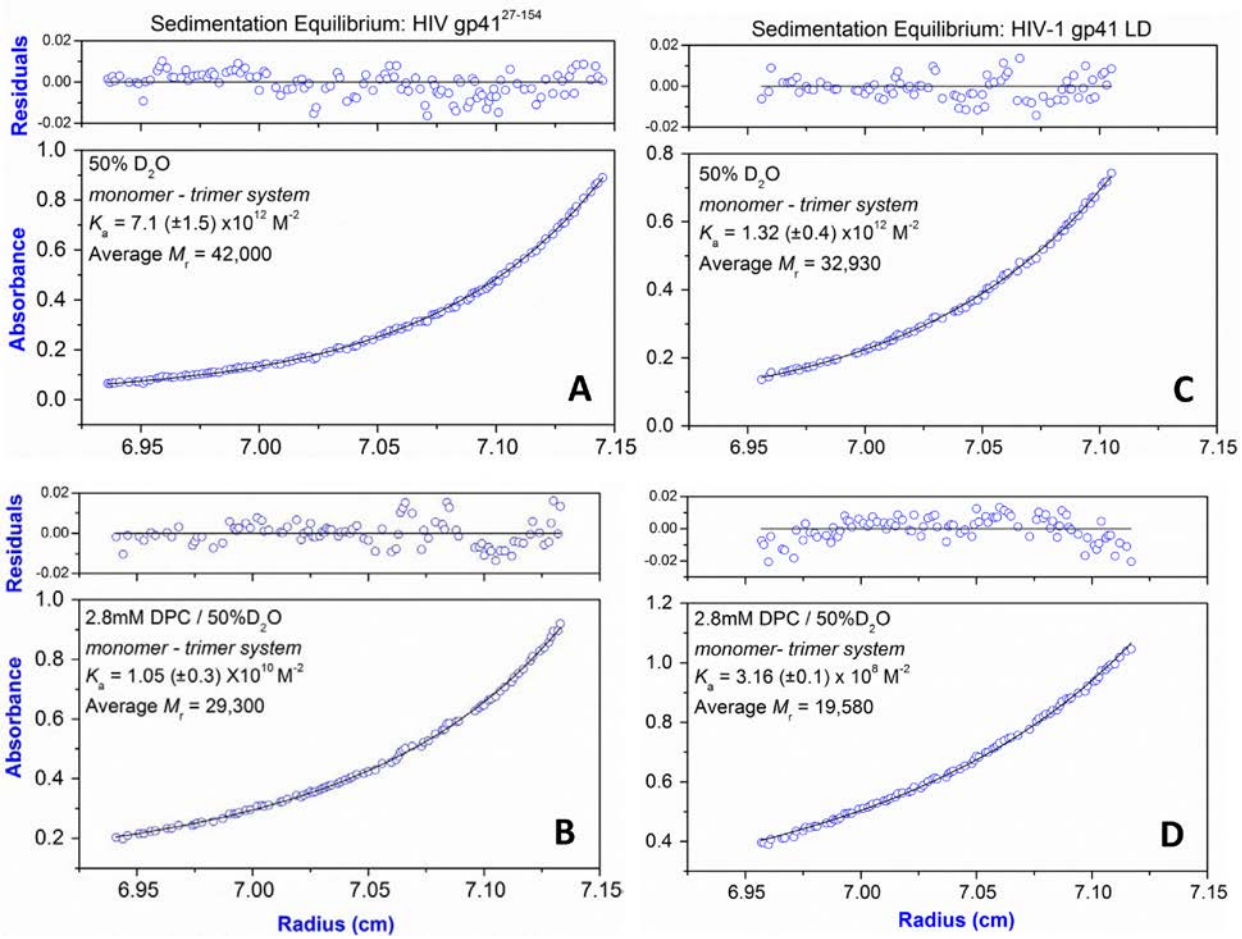

Figure S1.

Analytical Ultracentrifugation (relates to Results section "Monomer-Trimer Equilibrium" and Figure 4).

Sedimentation equilibrium data of the HIV-1 ectodomain gp41$^{27-154}$ in the absence of detergent (A) and in the presence of dodecyl phosphocholine (DPC, B) are shown. For comparison a loop deletion mutant (gp41 LD) of the gp41 ectodomain has been studied where the immunodominant loop region has been replaced by a six residue flexible linker. The monomer-trimer equilibrium has been analyzed in the absence (C) and presence of DPC (D). Panels are absorbance (bottom panel) and residuals (upper panel). Opened circles show 280nm absorbance gradients in the centrifuge cell. The solid line indicates the calculated fit for the monomer-trimer association. Residuals show the difference in the fitted and experimental values as a function of radial position. The average molecular weights were fitted using an ideal single species model (not shown) which made no assumptions about associative behavior.

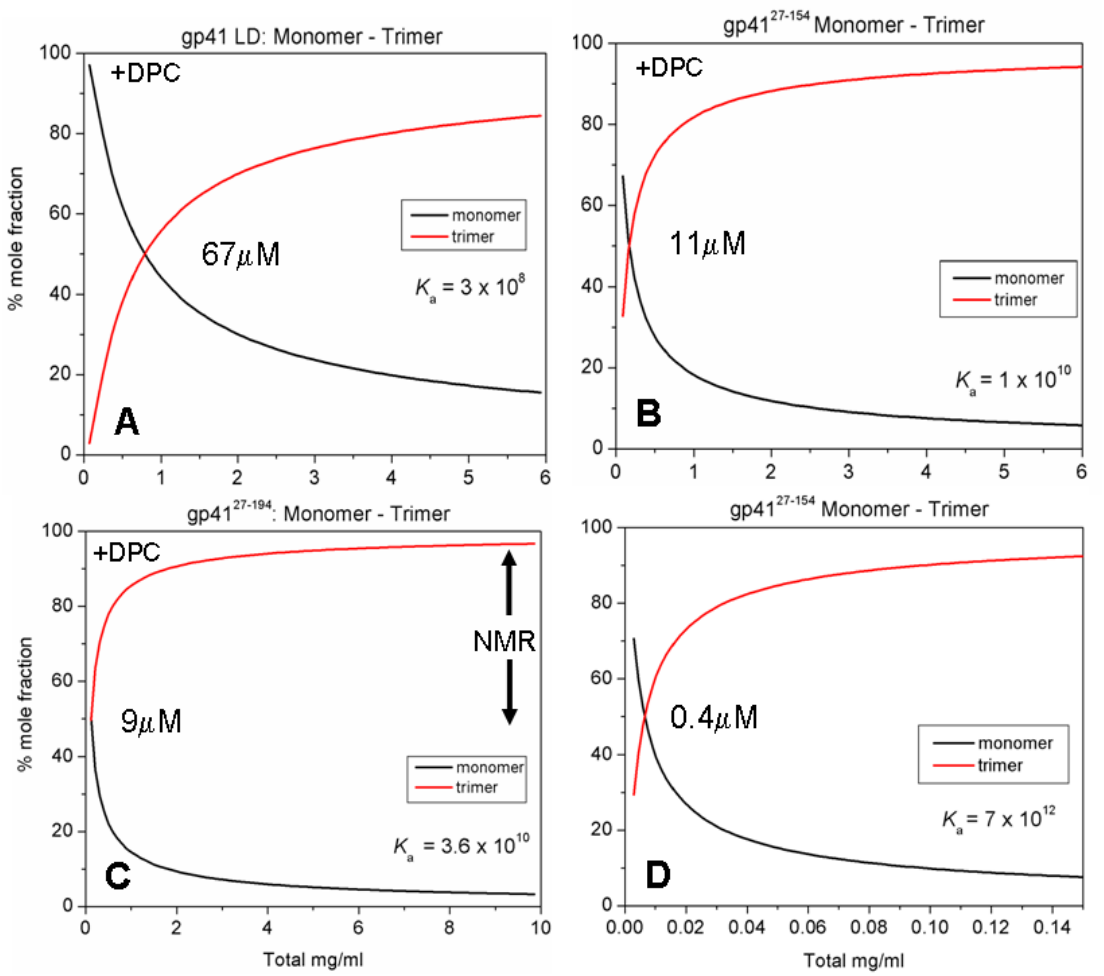

Figure S2.

Profiles of mole fraction of monomer and trimer species plotted as function of total protein concentration (related to the Results "Monomer-Trimer Equilibrium" and Figure 4)**.**

The concentration profiles were constructed using the K_a values indicated and which were derived from sedimentation equilibrium measurements (Figure 4 and Figure S1). Panels A-C, refer to K_a values derived from centrifugation performed in the presence of DPC and Panel D, in the absence of DPC. Panel A, gp41 LD (where IL in gp41$^{27-154}$ was replaced with 6 residue flexible linker): 11.83 kDa (1mg/ml = 84.5μM); Panel B, gp41$^{27-154}$: 14.90 kDa (1mg/ml = 67μM); Panel C, gp41$^{27-194}$: 19.65 kDa (1mg/ml = 50.9μM); Panel D, same as B. In all panels, the concentration (μM) corresponding to ~ 50% monomer ~ 50% trimer is indicated.

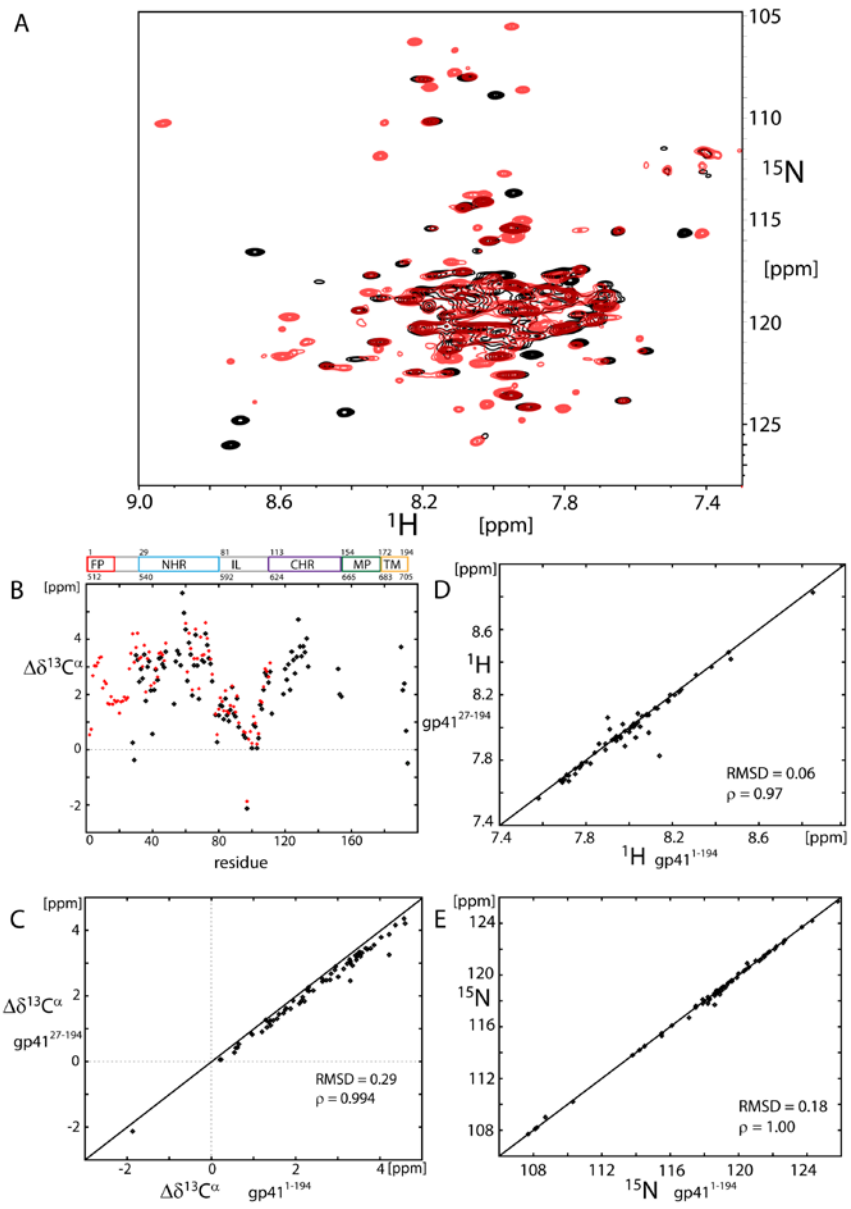

Figure S3.

Comparison of chemical shifts for gp41$^{27\text{-}194}$ and gp41$^{1\text{-}194}$ (comprising FP and FPPR), related to the Results section "Comparison of gp41$^{27\text{-}194}$ and gp41$^{1\text{-}194}$ including the fusion peptide" and Figure 1.

Comparison of chemical shifts: **(A)** Overlay of 800 MHz ^{15}N-^{1}H TROSY-HSQC spectra of ^{2}H^{15}N^{13}C enriched gp41$^{27\text{-}194}$ (black) and gp41$^{1\text{-}194}$ (red) (Lakomek et al., 2013). **(B)** $\Delta\delta^{13}C^{\alpha}$ secondary chemical shifts of gp41$^{1\text{-}194}$ (red) are compared to those of gp41$^{27\text{-}194}$ (black). **(C)** Correlation graph of $\Delta\delta^{13}C^{\alpha}$ values for residues 30-110 of gp41$^{1\text{-}194}$, comparing values measured for gp41$^{27\text{-}194}$. $\Delta\delta^{13}C^{\alpha}$ correlate very well between gp41$^{27\text{-}194}$ and gp41$^{1\text{-}194}$ but are slightly reduced in magnitude for gp41$^{27\text{-}194}$. **(D)** Correlation graph of ^{1}H chemical shifts of residues 32-110 of gp41$^{27\text{-}194}$, comparing values measured for gp41$^{1\text{-}194}$. **(E)** Correlation graph of ^{15}N chemical shifts of residues 31-110 of gp41$^{27\text{-}194}$, comparing values measured for gp41$^{1\text{-}194}$.

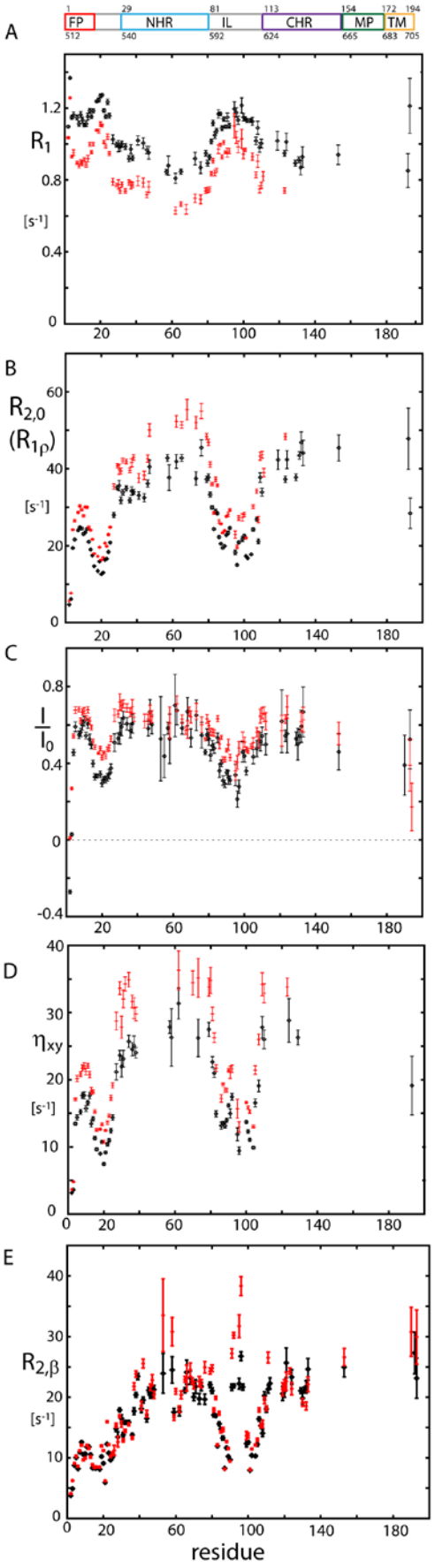

Figure S4

Extended analysis of gp41$^{1\text{-}194}$ relaxation data (relates to Results section "Comparison of gp41$^{27\text{-}194}$ and gp41$^{1\text{-}194}$ including the fusion peptide" and Figure 2).

^{15}N relaxation data recorded for gp41$^{1\text{-}194}$ in DPC micelles (Lakomek et al., 2013); additional resonances in the 2D spectra could be assigned based on comparison to gp41$^{27\text{-}194}$: **(A)** ^{15}N R_1 relaxation data at 600 MHz (black) and 800 MHz (red) are highly consistent for both fields. **(B)** $R_{2,0}$ relaxation data (derived from $R_{1\rho}$ with a 2 kHz RF field; R_1 contribution corrected) at 600 MHz (black) and 800 MHz (red). **(C)** ^{15}N-{^{1}H} NOE values. **(D)** Transverse CSA–dipolar cross-correlated relaxation rates η_{xy}. **(E)** ^{15}N $R_{2,\beta}$. Errors have been calculated from Monte-Carlo simulations (A,B) and error propagation of the spectral noise level (C-E).

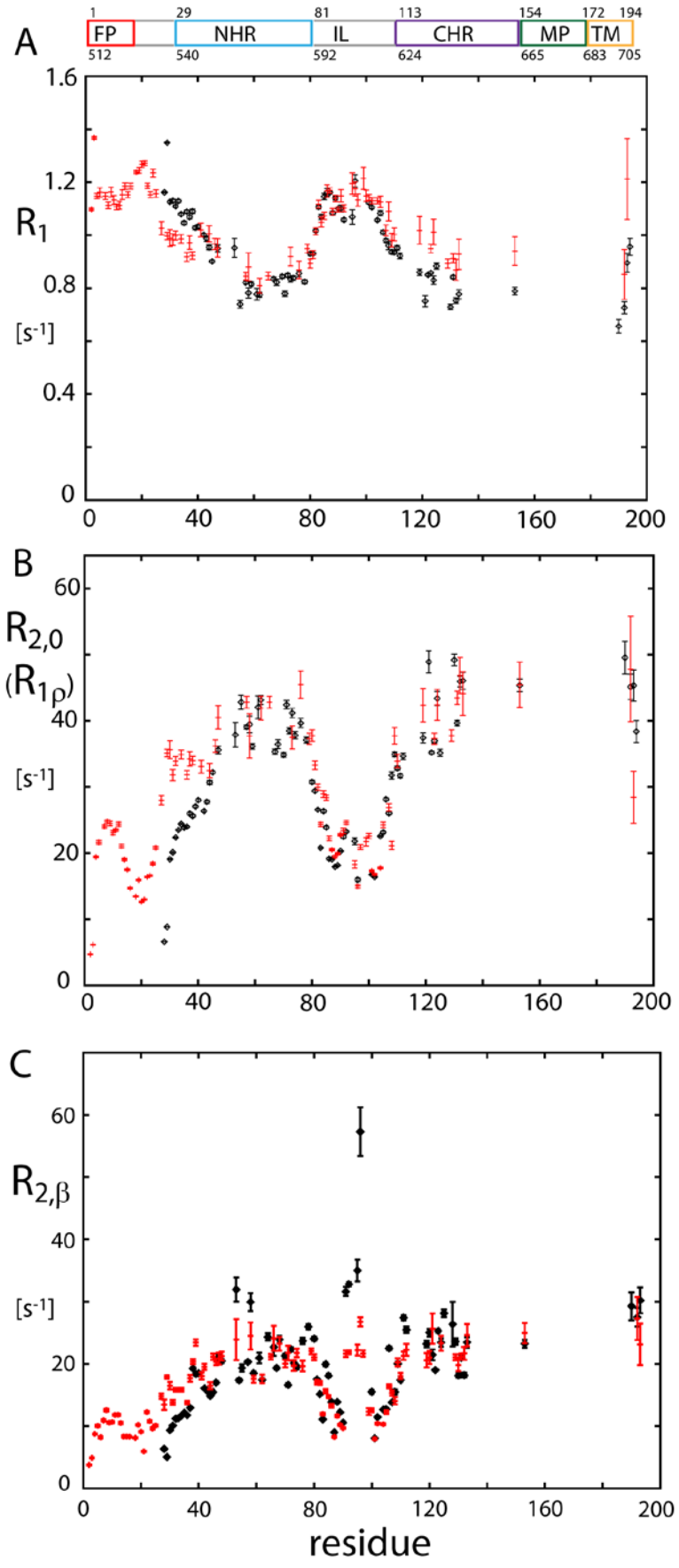

Figure S5

Comparison of ^{15}N relaxation data recorded at 600 MHz for gp41$^{1\text{-}194}$ in DPC micelles (red) (Lakomek et al., 2013) compared to rates measured for gp41$^{27\text{-}194}$ (black), related to Figure 2.

Panel **(A)** shows ^{15}N R_1, **(B)** ^{15}N $R_{2,0}$ relaxation data (derived from $R_{1\rho}$ with a 2 kHz RF field; R_1 contribution corrected), **(C)** ^{15}N $R_{2,\beta}$. Relaxation data for gp41$^{1\text{-}194}$ are very similar compared to gp41$^{27\text{-}194}$, major differences occur only for residues V28-R45 which are N-terminal in gp41$^{27\text{-}194}$, we, thus, consider them as a result of truncation. Errors have been calculated from Monte-Carlo simulations (A,B) and error propagation of the spectral noise level (C).

$\Delta\delta^{13}C^{\alpha}$ secondary chemical shift

Table S1. $\Delta\delta^{13}C^{\alpha}$ secondary chemical shift for $gp41^{27\text{-}194}$ (related to the Results section "Secondary structure analysis" and Figure 1).

AA	$\Delta\delta^{13}C^{\alpha}$	AA	$\Delta\delta^{13}C^{\alpha}$
	[ppm]		[ppm]
V28	0.25	G86	1.04
Q29	-0.38	A87	1.44
A30	3.42	S88	2.27
R31	3.25	G89	1.31
Q32	2.46	K90	1.20
L33	2.93	L91	1.86
L34	2.58	I92	0.82
S35	3.45	T95	0.53
G36	1.77	A96	0.43
I37	3.00	V97	-2.13
V38	3.20	N100	0.06
Q39	2.15	A101	0.91
Q40	0.57	S102	0.84
Q41	2.16	W103	0.06
N42	2.90	S104	0.42
N43	2.53	N105	1.63
L44	3.31	K106	1.47
L45	3.34	S107	2.17
R46	3.10	L108	2.79
A47	2.98	E109	2.67
I48	3.55	Q110	2.44
H53	1.66	I111	2.83
L54	3.20	W112	1.30
L55	3.58	E119	2.02
Q56	3.46	W120	2.92
L57	3.06	D121	2.54
T58	5.67	R122	3.09
V59	4.95	E123	2.17
W60	4.36	I124	3.55
G61	2.49	N125	3.25
I62	3.87	N126	2.76
K63	3.45	Y127	3.36
Q64	1.96	T128	4.71
L65	3.06	S129	3.74
Q66	4.16	L130	3.38

A67	3.05	I131	3.74
R68	1.84	H132	3.53
L70	3.23	S133	4.03
A71	3.18	L134	3.01
V72	4.21	L152	2.93
E73	3.79	D153	2.01
R74	3.31	K154	1.92
Y75	3.11	V190	3.72
L76	2.48	L191	2.16
D78	1.27	S192	2.40
Q79	0.27	I193	0.68
Q80	1.25	V194	-0.49
L81	1.61		
L82	1.58		
G83	1.10		
I84	1.85		
W85	1.25		
G86	1.04		

Extended Model-free Analysis

Table S2. Input experimental data for the Extended Model-free analysis and back-calculated data for quality assessment of the fit (this table is related to the Results section "Inter-domain dynamics" and Table 1). Average experimental data and error-weighted standard deviation for clusters of residues with similar dynamic properties in gp41$^{27\text{-}194}$ that were used as input for the extended model-free analysis are shown (Input). Back-calculated relaxation data are shown (Back-calculated) that were calculated using the model-free parameters shown in Table 1.

Input								
Cluster	R_1 [s^{-1}] 600 MHz	R_1 [s^{-1}] 800 MHz	R_2 [s^{-1}] 600 MHz	R_2 [s^{-1}] 800 MHz	I/I_0 600 MHz	I/I_0 800 MHz	η_{xy} [s^{-1}] 600 MHz	η_{xy} [s^{-1}] 800 MHz
55-78	0.81 ±0.04	0.61 ±0.03	39.1 ±2.8	49.0 ±3.8	0.63 ±0.06	0.71 ±0.05	27.7 ±3.1	35.7 ±2.8
83-102	1.12 ±0.04	0.95 ±0.04	20.2 ±3.0	24.2 ±3.6	0.39 ±0.07	0.50 ±0.06	13.5 ±2.5	17.4 ±2.7
119-133	0.81 ±0.05	0.62 ±0.05	41.8 ±5.3	50.7 ±5.3	0.59 ±0.06	0.67 ±0.05	30.1 ±5.1	32.4 ±3.4
190-194	0.81 ±0.13	0.66 ±0.09	44.6 ±4.6	47.6 ±2.0	0.54 ±0.10	0.56 ±0.11	28.2 ±4.1	40.1 ±3.7
Back-calculated								
55-78	0.80 ±0.03	0.63 ±0.02	38.2 ±1.5	46.9 ±1.8	0.67 ±0.04	0.69 ±0.04	29.0 ±1.1	38.5 ±1.5
83-102	1.11 ±0.03	0.96 ±0.04	19.2 ±1.5	23.4 ±1.9	0.42 ±0.05	0.46 ±0.03	14.5 ±1.2	19.2 ±1.6
119-133	0.80 ±0.04	0.64 ±0.04	37.3 ±1.9	45.7 ±2.3	0.62 ±0.04	0.65 ±0.04	28.3 ±1.4	37.6 ±1.9
190-194	0.75 ±0.07	0.64 ±0.07	39.0 ±1.4	47.9 ±1.7	0.55 ±0.06	0.62 ±0.07	29.6 ±1.1	39.4 ±1.4

NMR backbone assignment data

Table S3. Chemical shift assignments for the studied gp41$^{27\text{-}194}$ construct in DPC micelles (related to the Experimental Procedures section “NMR spectroscopy” and Figure 1). The table is provided as a separate Exel document.

^{15}N Relaxation data

Table S4A. ^{15}N R_1, ^{15}N $R_{2,0}$ (derived from ^{15}N $R_{1,\rho}$), {1H}-^{15}N NOE, transverse ^{15}N CSA –dipolar cross-correlated relaxation data η_{xy} and ^{15}N $R_{2,\beta}$ relaxation data for gp41$^{27\text{-}194}$, measured at 600 MHz and 800 MHz. This table is related to the Results section “Inter-domain dynamics” and Figure 2) and provided as a separate Exel document.

Lipid- and solvent PRE measurements

Table S5. Lipid (5-DSA) and solvent (Omniscan) PRE data. Intensities are normalized relative to a reference sample of identical gp41 and DPC concentration (related to Figure 3).

	I/I_0	$\Delta I/I_0$	I/I_0	$\Delta I/I_0$
	5-DSA		Omniscan	
V28	0.46	0.01	0.3	0.01
Q29	0.55	0.01	0.34	0.01
A30	0.56	0.02	0.44	0.01
R31	0.81	0.02	0.58	0.02
Q32	0.86	0.01	0.61	0.01
L33	0.76	0.01	0.66	0.01
L34	0.69	0.01	0.74	0.01
S35	0.76	0.02	0.69	0.02
G36	0.76	0.01	0.58	0.01
I37	0.75	0.02	0.73	0.02
V38	0.76	0.02	0.72	0.02
Q39	0.70	0.02	0.69	0.02
Q40	0.86	0.02	0.6	0.02
N42	0.85	0.02	nd	nd
N43	0.93	0.03	0.51	0.02
L44	0.54	0.02	0.61	0.02
R46	0.87	0.03	0.77	0.03
A47	0.78	0.02	0.73	0.02
I48	0.82	0.02	0.76	0.02
H53	0.76	0.05	nd	nd
L54	0.73	0.02	0.67	0.02
L57	0.85	0.02	nd	nd
T58	0.76	0.05	0.65	0.05
V59	0.74	0.02	0.74	0.02
G61	0.72	0.05	0.67	0.05
I62	0.62	0.02	0.73	0.02
Q64	0.79	0.02	0.58	0.02
L65	0.70	0.02	0.54	0.01
Q66	0.55	0.03	0.7	0.03
A67	0.50	0.01	nd	nd
L70	0.70	0.02	0.67	0.02
A71	0.82	0.03	0.7	0.03
E73	0.57	0.02	0.55	0.02
R74	0.90	0.02	0.48	0.01
Y75	0.73	0.03	0.5	0.02
L76	0.87	0.02	0.77	0.02

D78	0.70	0.02	0.52	0.02
L81	0.76	0.01	0.6	0.01
L82	0.67	0.02	0.62	0.02
G83	0.44	0.02	0.54	0.02
I84	0.68	0.02	0.67	0.02
W85	0.64	0.02	0.64	0.02
G86	0.48	0.02	0.52	0.02
A87	0.66	0.01	0.5	0.01
S88	0.73	0.01	0.46	0.01
G89	0.74	0.02	0.47	0.01
K90	0.82	0.01	0.55	0.01
L91	0.62	0.01	0.7	0.01
I92	0.75	0.01	0.66	0.01
T95	0.66	0.02	0.55	0.02
A96	0.54	0.01	0.54	0.01
V97	0.59	0.02	0.58	0.02
N100	0.44	0.03	0.53	0.03
A101	0.62	0.01	0.41	0.01
W103	0.75	0.02	nd	nd
S104	0.66	0.01	0.43	0.01
N105	0.66	0.03	nd	nd
S107	0.73	0.02	0.44	0.01
L108	0.47	0.03	0.52	0.03
Q109	0.74	0.03	0.55	0.02
Q110	0.82	0.02	0.5	0.02
D121	0.69	0.04	0.51	0.04
I124	0.69	0.03	0.64	0.03
N125	0.78	0.02	0.53	0.02
N126	0.88	0.01	0.45	0.01
T128	0.81	0.05	nd	nd
S129	nd	nd	0.51	0.02
L130	0.87	0.02	0.59	0.02
I131	0.81	0.01	0.66	0.01
H132	0.75	0.02	0.7	0.02
S133	0.85	0.03	0.59	0.02
L134	0.49	0.02	0.41	0.02
D153	0.84	0.03	0.56	0.03
V190	0.66	0.04	0.77	0.04
L191	0.78	0.01	0.61	0.01
S192	0.59	0.04	0.51	0.03
I193	0.71	0.04	0.61	0.04
V194	0.58	0.04	0.37	0.04

Supplemental References

Lakomek, N.A., Kaufman, J.D., Stahl, S.J., Louis, J.M., Grishaev, A., Wingfield, P.T., and Bax, A. (2013). Internal Dynamics of the Homotrimeric HIV-1 Viral Coat Protein gp41 on Multiple Time Scales. Angew Chem Int Edit *52*, 3911-3915.